Density Functional Theory Study of Thermodynamic and Kinetic Isotope Effects of H2/D2 Dissociative Adsorption on Transition Metals

Catalysis Science & Technology

Density Functional Theory Study of Thermodynamic and Kinetic Isotope Effects of H₂/D₂ Dissociative Adsorption on Transition Metals

Yunhai Bai[+], Benjamin W. J. Chen[+], Guowen Peng, Manos Mavrikakis*

Department of Chemical and Biological Engineering, University of Wisconsin – Madison,

Madison, WI 53706

[+] = contributed equally to this work

*corresponding author emavrikakis@wisc.edu

Keywords: density functional theory; H₂ dissociative adsorption, D₂ dissociative adsorption, thermodynamic isotope effect, kinetic isotope effect

ABSTRACT

We studied the thermodynamic isotope effects (TIEs) and kinetic isotope effects (KIEs) for H₂/D₂ dissociative adsorption using periodic, density functional theory (DFT) -based calculations. We examined the TIEs on the close–packed, open, and stepped surfaces, of twelve transition metals (Fe, Co, Ni, Cu, Ru, Rh, Pd, Ag, Re, Ir, Pt, and Au), and the KIEs on the surfaces of three noble metals (Cu, Ag, and Au). Both TIEs and KIEs were evaluated at 1/9 ML coverage. We find distinct TIEs on different adsorption sites, indicating that TIEs could be used in conjunction with binding energies to determine the dominant adsorption sites for hydrogen. Additionally, we find that while H₂ dissociative adsorption may traditionally be considered structure insensitive in terms of reaction rates, it can exhibit structure sensitivity in terms of its KIEs. Complementarily to TIEs, KIEs might therefore be useful for identifying active sites for H₂ dissociative adsorption on the three noble metal transition metal catalysts studied.

1

1. Introduction

Hydrogen/Deuterium (H/D) isotope effects are very useful for probing the mechanisms of chemical reactions involving H atoms in their elementary steps – for example, CO hydrogenation and methane reforming,[1–7] alkene and arene hydrogenation,[8–14] and other hydrogen transfer reactions.[15–17] Previously, we studied H_2/D_2 isotope effects in Fischer–Tropsch synthesis on Fe(110) and Co(0001) at high CO coverages.[1] Experimentally, inverse kinetic isotope effects (KIEs) ($r_H/r_D < 1$, where r_X refers to the rate of reaction using isotope X) were observed. From a combination of experiment and density functional theory (DFT) -based calculations, we were able to deduce that these inverse KIEs were due to a convolution of the isotope effects experienced by the quasi-equilibrated steps before the rate determining steps (RDSs).[1] From these results, we were also able to confirm the prevalence of H–assisted CO dissociation routes on both Fe and Co catalysts for Fisher–Tropsch synthesis, demonstrating that theoretically calculated isotope effects based on DFT can be useful for probing mechanistic pathways.[1]

As highlighted above, and depending on the reaction mechanism and the location of the RDSs along the reaction pathway, experimentally observed KIEs may be an aggregate effect of the TIEs and KIEs of several elementary steps.[1,18] It is thus often premature to make unequivocal mechanistic conclusions based solely on the overall observed KIE. Thorough knowledge about the magnitudes and nature (whether inverse or normal) of the KIEs and TIEs for each proposed elementary step in the mechanism is vital.

Compared to the abundance of experimental literature on H/D isotope effects, theoretical studies are relatively scarce. Here, using DFT-based calculations, we study the TIEs of H_2/D_2 dissociative adsorption on transition metal surfaces, a critical process for generating atomic H for

other chemical reactions. We systematically go through different possible adsorption sites (which present different binding energies and vibrational modes) for atomic H/D, and calculate the expected TIEs assuming adsorption on these sites. Based on the energetic stability of these sites for adsorption of H/D, we can then predict the TIEs that would be experimentally observed if H_2/D_2 dissociative adsorption were to be studied on a particular transition metal surface.

In total, 28 different transition metal surfaces, comprising 12 close–packed surfaces (fcc(111), hcp(0001), and bcc(110)), 8 open fcc(100) surfaces, and 8 stepped fcc(211) surfaces, are studied. We further examine the kinetic isotope effects (KIEs) of H_2/D_2 dissociative adsorption on the (111), (100), and (211) surfaces of 3 noble metals (Cu, Ag, and Au), where dissociation is activated. Importantly, we also study the temperature dependence of TIEs and KIEs on these metal surfaces.

2. Computational Methods

All calculations were performed using the Vienna ab–initio Simulation Package (VASP).[19,20] Projector augmented–wave (PAW) pseudopotentials[21,22] were used to describe the nuclei and core electrons, while the wavefunctions of the valence electrons were expanded using plane waves with an energy cutoff of 400 eV. Exchange–correlation contributions to the potential and total energy were included using the generalized gradient approximation of Perdew and Wang (GGA–PW91).[23] To assess the dependence of the results on the functional used, we performed trial calculations with the PBE+D3,[24] and optb88-vdW functionals[25,26] on Ru, Pt, and Ir. A maximum spread of 0.02 in the TIEs of H_2 dissociation was observed. Therefore, the PW91 functional was deemed adequate for this work. Recent studies on the accuracy of different functionals for bulk properties of transition metal systems, such as lattice constants and surface

energies, also show that PW91 is among one of the most accurate functionals available for these properties,[27–29] providing further support for our choice of functional.

The close–packed surfaces (fcc(111), hcp(0001), and bcc(110) surfaces) and open surfaces (fcc(100)) were modeled by (3×3) five–layer and six–layer slabs, respectively, corresponding to 1/9 monolayer (ML) coverage for a single H atom in the unit cell. The top three (four) layers of the close (open)–packed surfaces were relaxed. A 6×6×1 Monkhorst–Pack k–point mesh[30] was used to sample the first Brillouin zone of the close–packed and open surfaces except for Cu(111), Ag(111), and Au(111), where a denser 8×8×1 Monkhorst–Pack k–point mesh was used instead. The stepped (211) surfaces were modeled by a twelve–layer slab in a (1×3) surface unit cell. The top seven layers were relaxed. An 8×6×1 Monkhorst–Pack k–point mesh was used to sample the first Brillouin zone of the (211) − (1×3) stepped surfaces.

Successive slabs were separated by a vacuum region of ~12 Å in the z–direction. Adsorption was allowed on only one of the two exposed metal surfaces, with the electrostatic potential adjusted accordingly.[31,32] Convergence with respect to various computational parameters was verified. All structures were fully relaxed until the Hellmann–Feynman forces acting on the atoms were smaller than 0.02 eV / Å. For Co, Ni, and Fe surfaces, spin–polarized calculations were performed.

Minimum energy paths and activation energy barriers were calculated using the climbing image nudged elastic band (CI–NEB) method.[33] The transition state for each path was confirmed by a single imaginary frequency in the vibrational frequency calculations.

The binding energy (B.E.) is defined as B.E. $= E_{ads} - E_{clean} - E_{gas}$, where E_{ads}, E_{clean} and E_{gas} are the total energies of the slab with an adsorbate, the clean slab, and the adsorbate species in the gas phase, respectively. A negative B.E. reflects exothermic binding. Note that the potential energy surfaces for adsorption of H and D are the same, and therefore to assess their most stable binding sites at 0 K, we calculated the zero–point energy (ZPE) corrections to the B.E. (see below), which are different for H and D.

Vibrational frequencies were calculated by numerical differentiation of the forces using a second–order finite difference approach with a step size of 0.015 Å. The frequencies were converged with respect to the step size. The Hessian matrix was mass–weighted and diagonalized to yield the normal mode frequencies.

The ZPE correction was calculated according to Equation (1),

$$ZPE = \frac{hc}{2} \sum_i^3 \frac{1}{\lambda_i}, \tag{1}$$

where h is the Planck constant, c the speed of light, and λ_i the wavelength corresponding to the i–th vibrational mode.

The vibrational entropy S_{vib} was calculated assuming that each mode behaves as a harmonic oscillator, as shown in Equation (2),

$$S_{vib} = R \sum_i^6 \left(\frac{x_i}{e^{x_i} - 1} - \ln(1 - e^{-x_i}) \right), \tag{2}$$

where $x_i = \frac{hc}{k_B T} \frac{1}{\lambda_i}$, R is the ideal gas constant, k_B the Boltzmann constant, and T the reaction temperature.

We note that the harmonic oscillator approximation may not be valid under all conditions. The small mass of H, when coupled with flat potential energy surfaces (PESs), promotes quantum delocalization of H parallel to the surface.[34] On Ni(111), Christmann et al. noted that since the thermal de Broglie wavelength for H of 1 Å was in the order of magnitude of the Ni–Ni separation, the states of motion parallel to the surface might be better described by an extended atomic band structure of Bloch waves created by the diffraction of H off the lattice.[35] This was also observed on Rh(111), where using high resolution electron energy loss spectroscopy (HREELS), Somorjai et al. noticed quantum delocalization of H in directions parallel to the surface.[36] In these cases only motion perpendicular to the surface should be approximated as a harmonic oscillator.

The harmonic oscillator approximation may also fail when the thermal energy kT, where k is the Boltzmann constant, is greater than the barrier for diffusion of H, in which case the adsorption of H is better described as a 2D gas.[37,38] Small vibrational frequencies, for example, for H adsorbed at certain top sites, combined with high temperatures, may thus lead to larger errors from the harmonic oscillator approximation. However, we note here that most of the frequencies we have calculated are large (> 250 cm^{-1}) and for these cases the harmonic oscillator approximation should be reasonably accurate.

Additionally, quantum tunneling of H has been shown to affect rates of many reactions, including hydrogen dissociation.[39–41] However, these effects would be significant only at low temperatures.

The entropy of a gas phase molecule consists of vibrational, three–dimensional (3D) translational, and rotational contributions. The vibrational entropy was calculated using Equation

(2), while the 3D translational and rotational contributions to the total entropy were obtained with Equations (3) and (4), respectively,

$$S_{trans}^{3D} = R \left\{ \ln\left[\left(\frac{2\pi m k_B T}{h^2} \right)^{3/2} \frac{k_B T}{P} \right] + 2.5 \right\}, \tag{3}$$

$$S_{rot,linear} = R \left\{ \ln\left[\frac{8\pi^2 I_{max} k_B T}{s_{number} h^2} \right] + 1.5 \right\}, \tag{4}$$

where m is the molecular mass, P the pressure, I_{max} the principal moment of inertia, and s_{number} the symmetry number of the molecule (2 for H_2 and D_2).

The thermodynamic isotope effect (TIE) for H_2/D_2 dissociative adsorption was calculated with Equations (5) and (6),

$$K_{eq} = \exp\left\{ \left(-\frac{1}{RT} \right) \left(\Delta H^{FS-IS} - T\Delta S^{FS-IS} \right) \right\}, \tag{5}$$

$$\text{TIE} \equiv \frac{K_{eq}^H}{K_{eq}^D} \approx \left[\frac{K_{eq}^H}{K_{eq}^D} \right]_{ZPE} \left[\frac{K_{eq}^H}{K_{eq}^D} \right]_S = \text{TIE}_{ZPE}\, \text{TIE}_S$$

$$= \exp\left\{ \left(-\frac{1}{RT} \right) [\Delta H_H - \Delta H_D] \right\} \exp\left\{ \frac{1}{R} [\Delta S_H - \Delta S_D] \right\}$$

$$\approx \exp\left\{ \left(-\frac{1}{RT} \right) \left[(\text{ZPE}_H^{FS} - \text{ZPE}_H^{IS}) - (\text{ZPE}_D^{FS} - \text{ZPE}_D^{IS}) \right] \right\} \exp\left\{ \frac{1}{R} \left[(S_H^{FS} - S_H^{IS}) - (S_D^{FS} - S_D^{IS}) \right] \right\}, \tag{6}$$

where K_{eq} is the equilibrium constant, ΔH is the reaction enthalpy, and $\text{TIE}_{ZPE} / \text{TIE}_S$ are the ZPE and entropic contributions to the TIE respectively. Initial state (gas phase H_2/D_2) and final state (adsorbed H/D) terms are denoted by the superscripts IS and FS respectively. The final state with 2 adsorbed H/D is assumed to be at infinite separation. As done in our previous work, we consider finite temperature corrections to the enthalpy as negligible.[1]

The kinetic isotope effect (KIE) for H_2/D_2 dissociative adsorption was calculated similarly with Equation (7),

$$\text{KIE} \equiv \frac{k_H}{k_D} \approx \left[\frac{k_H}{k_D}\right]_{\text{ZPE}} \left[\frac{k_H}{k_D}\right]_{\text{S}} = \text{KIE}_{\text{ZPE}}\,\text{KIE}_{\text{S}}$$

$$\approx \exp\left\{\left(-\frac{1}{RT}\right)\left[(\text{ZPE}_H^{\text{TS}} - \text{ZPE}_H^{\text{IS}}) - (\text{ZPE}_D^{\text{TS}} - \text{ZPE}_D^{\text{IS}})\right]\right\} \exp\left\{\frac{1}{R}\left[(S_H^{\text{TS}} - S_H^{\text{IS}}) - (S_D^{\text{TS}} - S_D^{\text{IS}})\right]\right\}, \quad (7)$$

where k is the rate constant, and KIE_{ZPE} / KIE_{S} are the ZPE and entropic contributions to the kinetic isotope effect, respectively. The superscript TS denotes a transition state. Similar to the calculations of the TIE, we have neglected finite temperature corrections to the enthalpy.

3. Results and Discussion

This section is organized as follows: we will first present thermodynamic isotope effects (TIEs) for H_2/D_2 dissociative adsorption on the close–packed surfaces in section (A). Then we will discuss TIEs on open (100) surfaces and stepped (211) surfaces in sections (B) and (C), respectively. In section (D), we will discuss kinetic isotope effects (KIEs) for the same reaction on the noble metal surfaces. Finally, an analysis of the temperature dependence of TIEs and KIEs will be presented in section (E).

A. TIEs on close–packed surfaces

For fcc and hcp metals, the binding of H/D on the four high symmetry sites: fcc, hcp, bridge, and top sites, was investigated. For Fe, a bcc metal, the hollow, s–bridge, l–bridge, and top sites were considered. For an explanation of site nomenclature on hcp(0001), bcc(110), and fcc(111) surfaces, see **Figures 1(a) – (c)**. The TIEs for H_2/D_2 dissociative adsorption, assuming binding at each of these different high symmetry sites, were then calculated.

The binding energies (B.E.), zero-point energy corrected binding energies (B.E. + ZPE), vibrational frequencies (v), zero–point energies (ZPE), entropies (S), for H/D adsorption at low–coverage (θ = 1/9 ML) on different close–packed surfaces, and the TIEs for H_2/D_2 dissociative adsorption, including their breakdown into ZPE and entropy contributions, are summarized in **Table 1**. All entropies are calculated at 623 K. The most stable adsorption site on each surface is indicated with bold font.
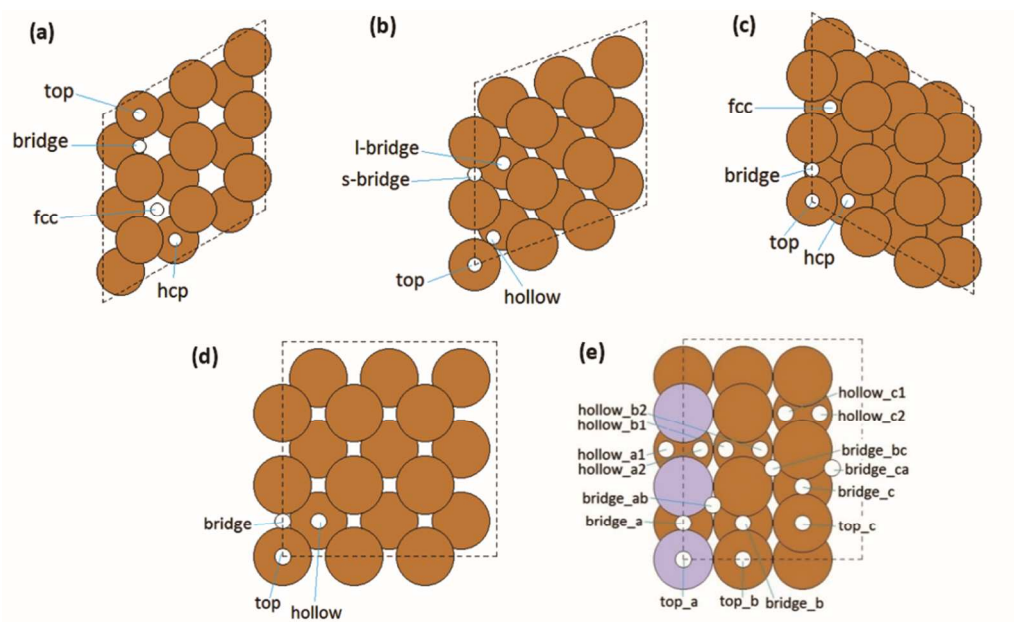
Figure 1. Top views of high symmetry adsorption sites for atomic hydrogen on (a) hcp(0001), (b) bcc(110), (c) fcc(111), (d) fcc(100), and (e) fcc(211) surfaces. Filled circles denote the surface atoms, and open circles denote high symmetry sites. Atoms in light purple (in (e)) highlight the step edge.

Table 1 Calculated binding energies (B.E., eV), zero-point energy corrected binding energies (B.E. + ZPE, eV), vibrational frequencies (ν, cm^{-1}), zero–point energies (ZPE, eV), and entropies (S, J/mol/K) for H/D adsorption, as well as ZPE contributions (TIE–ZPE), entropic contributions (TIE–S) to the overall thermodynamic isotope effects (TIE–Overall) for H_2/D_2 dissociative adsorption at 623 K and a coverage of 1/9 ML on close–packed surfaces. Only stable sites are shown. Definitions of these terms can be found in the methods section. Experimental binding geometries, if available, are indicated.

Surface	Site	Expt. Site	B.E.	B.E.+ ZPE$_H$	B.E.+ ZPE$_D$	H[a] ν_H	ZPE$_H$	S$_H$[b]	D[a] ν_D	ZPE$_D$	S$_D$[b]	TIE ZPE	S	Overall
Re(0001)	**fcc**		−2.97	**−2.78**	**−2.84**	972, 976, 1095	0.19	8.8	685, 688, 772	0.13	15.1	**0.53**	**1.26**	**0.67**
	hcp		−2.93	−2.75	−2.80	885, 895, 1126	0.18	9.7	624, 631, 794	0.13	16.2	0.59	1.21	0.72
Fe(110)	**hollow**	H: hollow[42,43]	−3.00	**−2.83**	**−2.88**	760, 906, 1086	0.17	10.7	535, 639, 765	0.12	17.4	**0.64**	**1.15**	**0.74**
Ru(0001)	**fcc**	H: fcc[44,45] D: hollow[46]	−2.89	**−2.72**	**−2.77**	795, 798, 1105	0.17	11.1	561, 562, 744	0.12	17.9	**0.69**	**1.13**	**0.78**
	hcp		−2.82	−2.66	−2.71	733, 737, 1072	0.16	12.3	517, 519, 755	0.11	19.3	0.74	1.09	0.81
	top		−2.44	−2.31	−2.35	105, 124, 1867	0.13	39.5	74, 87, 1316	0.09	46.4	1.04	1.11	1.15
Co(0001)	**fcc**	H: fcc+hcp[47]	−2.83	**−2.65**	**−2.70**	882, 883, 1126	0.18	9.8	622, 622, 794	0.13	16.3	**0.59**	**1.20**	**0.71**
	hcp		−2.80	−2.63	−2.68	831, 833, 1122	0.17	10.5	586, 587, 791	0.12	17.2	0.64	1.16	0.74
Rh(111)	**fcc**	H: hollow[48] D: fcc[49] QD[d],36	−2.84	**−2.68**	**−2.73**	760, 764, 1088	0.16	11.8	536, 539, 767	0.11	18.6	**0.72**	**1.11**	**0.79**
	hcp		−2.81	−2.65	−2.70	727, 730, 1083	0.16	12.4	512, 515, 763	0.11	19.3	0.77	1.09	0.84
	top		−2.49	−2.35	−2.39	159, 163, 2001	0.14	33.6	112, 115, 1410	0.10	40.4	0.86	1.15	0.99
Ir(111)	fcc	H: top[50] QD[50]	−2.71	−2.56	−2.46	615, 619, 1128	0.15	14.4	433, 436, 795	0.10	21.6	0.86	1.04	0.90
	hcp		−2.68	−2.54	−2.58	547, 552, 1138	0.14	16.1	386, 389, 802	0.10	23.3	0.93	1.01	0.94
	top		−2.78	**−2.59**	**−2.65**	402, 405, 2173	0.19	18.7	283, 286, 1532	0.13	25.0	**0.55**	**1.27**	**0.70**
Ni(111)	**fcc**	H & D: fcc+hcp[43,51] QD[35,52]	−2.83	**−2.65**	**−2.70**	879, 882, 1125	0.18	9.8	619, 621, 793	0.13	16.4	**0.59**	**1.20**	**0.71**
	hcp		−2.82	−2.64	**−2.70**	857, 862, 1131	0.18	10.1	604, 607, 797	0.12	16.7	0.59	1.19	0.70
Pd(111)	**fcc**	H: fcc[53,54] QD[55]	−2.87	**−2.70**	**−2.75**	853, 863, 948	0.17	11.0	601, 608, 668	0.12	17.8	**0.69**	**1.12**	**0.77**
	hcp		−2.82	−2.66	−2.71	828, 837, 953	0.16	11.4	584, 590, 672	0.11	18.2	0.72	1.11	0.79
Pt(111)	**fcc**	H[56] and D[57]: fcc QD (below <0.75 ML)[58]	−2.76	**−2.62**	**−2.66**	633, 637, 1024	0.14	14.5	446, 449, 722	0.10	21.8	**0.89**	**1.02**	**0.91**
	hcp		−2.71	−2.58	−2.61	558, 558, 1053	0.13	16.2	393, 393, 742	0.10	23.6	1.00	0.99	0.99
	top		−2.76	−2.57	−2.63	379, 383, 2262	0.19	19.6	267, 270, 1594	0.13	25.8	0.53	1.28	0.68

Cu(111)	**fcc**	H: hollow[59]	−2.50	**−2.33**	**−2.38**	827, 831, 1046	0.17	10.9	583, 586, 737	0.12	17.7	**0.66**	**1.13**	**0.75**
	hcp		−2.50	**−2.33**	**−2.38**	824, 830, 1055	0.17	10.9	580, 585, 743	0.12	17.7	**0.66**	**1.14**	**0.75**
Ag(111)	**fcc**	H: hollow[60]	−2.12	**−1.98**	**−2.02**	718, 721, 828	0.14	14.1	506, 508, 584	0.10	21.4	**0.89**	**1.00**	**0.90**
	hcp		−2.12	**−1.98**	**−2.02**	699, 705, 845	0.14	14.3	493, 497, 596	0.10	21.6	**0.93**	**1.00**	**0.93**
Au(111)	**fcc**		−2.10	**−1.97**	**−2.01**	644, 648, 794	0.13	15.8	454, 456, 560	0.09	23.3	**1.04**	**0.96**	**0.99**
	hcp		−2.07	−1.94	−1.98	593, 596, 837	0.13	16.6	418, 420, 590	0.09	24.2	1.08	0.94	1.02
	top		−1.91	−1.76	−1.80	244, 247, 1988	0.15	26.7	172, 174, 1401	0.11	33.4	0.77	1.16	0.90

[a] Calculated ν, ZPE, and S for gas phase H_2 and D_2 at 0.1 atm are 4314 cm^{-1}, 0.27 eV, 175.0 J/mol/K and 3041 cm^{-1}, 0.19 eV, 189.6 J/mol/K, respectively. [b] All entropies were calculated at 623 K. [c] Items in bold indicate the calculated most stable sites on each surface. [d] QD denotes possible quantum delocalization of H parallel to the surface at low coverages.

As shown in **Table 1**, H generally prefers to bind at highly coordinated fcc and hcp sites; these sites are almost isoenergetic on all metals. There is however a slight preference for fcc sites, in good agreement with results reported previously.[61–73] Ir(111) is the only exception where H prefers to bind on the top site, in line with previous experimental and theoretical studies.[65,73] The preferred binding sites do not change upon correcting for the ZPE. The same conclusions apply for the adsorption of D; we do not observe any changes in the preferred adsorption site of D compared to H.

Remarkably, for most of the sites, inverse TIEs (i.e. $K_H/K_D < 1$) are found. The only two exceptions are the top site of Ru(0001) and the hcp site of Au(111), where TIEs larger than unity are found. Based on energetics, neither of these sites is predicted to be the most stable for H adsorption. We also note that the TIEs on hcp and fcc sites of different metals are very similar.

The TIE can be broken down into ZPE and entropic contributions. On the close–packed surfaces, the ZPE contributions are mostly less than unity (except for Ru(0001) top sites, Pt(111) hcp sites, Au(111) hollow sites); the ZPE contributions favor dissociation of D_2 over that of H_2. This is mainly due to the smaller ZPE of adsorbed D. This is evident from the more negative ZPE–corrected BEs for D compared to H.

On the other hand, the entropic contributions are mostly larger than unity, again with the notable exception of the hollow sites of Au(111). This means that dissociation of H_2 (g) is entropically more favorable than that of D_2 (g). We can rationalize this by noting that the entropy of D_2 (g) is much larger than that of H_2 (g) (by ~15 J mol^{-1} K^{-1} at 623 K), due mostly to the difference in translational entropy. However, the difference in vibrational entropy of D and H on metal surfaces is much smaller (only ~3–4 J mol^{-1} K^{-1} in favor of D at 623 K).

Notice that the ZPE and entropic contributions trend in opposite directions. Higher vibrational frequencies, such as M–H stretches on top sites, will lead to smaller ZPE contributions. However, they also lead to an increase in entropy contributions. These two components thereby partially compensate for each other even if the vibrational frequencies may vary significantly for different sites. Overall, as the entropic contribution is usually weaker (closer to unity), an inverse TIE effect is observed.

With the relatively wide range of predicted TIEs for different sites on each metal, we envision that the TIE could be a useful tool for determination of the preferred adsorption sites of H/D, given knowledge of the surface facets involved. This would work especially well for single crystal surfaces/nanoparticles which expose only one type of facet, and can be done simply by comparing the experimental and theoretical TIEs for different adsorption sites.

This can be particularly useful when standard binding energy calculations do not show an unambiguous preference for any one site. For example, whether H binds at top or fcc sites on Pt(111) is a very difficult question to answer using standard DFT-based calculations due to the closeness in the binding energies of H on these two sites.[58,69,74] However, the top site has a very different TIE (0.68) as compared to the fcc site (0.91), meaning that these binding sites can be easily differentiated if experimental measurements of the TIE are available.

B. TIEs on open fcc(100) surfaces

To study the structure sensitivity of H_2/D_2 dissociative adsorption TIEs, we calculated TIEs on the fcc(100) surfaces of 8 transition metals. Three high symmetry adsorption sites, bridge, hollow, and top sites, were studied for binding of H/D. Illustrations of the different sites are shown in **Figure 1(d)**. A summary of binding energies (B.E.), zero-point energy corrected

binding energies (B.E. + ZPE), vibrational frequencies (ν), zero–point energies (ZPE), and entropies (S) for H/D adsorption on fcc(100) surfaces at low–coverage (θ = 1/9 ML), as well as the TIEs for H_2/D_2 dissociative adsorption, including their breakdown into ZPE and entropic contributions, are given in **Table 2**.

Table 2 Calculated binding energies (B.E., eV), zero-point energy corrected binding energies (B.E. + ZPE, eV), vibrational frequencies (ν, cm^{-1}), zero–point energies (ZPE, eV), and entropies (S, J/mol/K) for H/D adsorption, as well as ZPE contributions (TIE–ZPE), entropic contributions (TIE–S) to the overall thermodynamic isotope effects (TIE–Overall) for H$_2$/D$_2$ dissociative adsorption at 623 K and a coverage of 1/9 ML on different fcc(100) surfaces. Only stable sites are shown. Definitions of these terms can be found in the methods section. Experimental binding geometries, if available, are indicated.

surface	site	Expt. Site	B.E	B.E.+ZPE$_H$	B.E.+ZPE$_D$	H[a]			D[a]			TIE		
						ν_H	ZPE$_H$	S_H[b]	ν_D	ZPE$_D$	S_D[b]	ZPE	S	Overall
Rh(100)	bridge	H[75] and D[76]: hollow	−2.80	−2.64	−2.69	245, 1002, 1300	0.16	17.9	172, 706, 916	0.11	24.6	0.76	1.14	0.87
	hollow		−2.77	**−2.70**	**−2.72**	218, 253, 729	0.07	31.9	154, 178, 514	0.05	40.1	**1.92**	**0.81**	**1.56**
Ir(100)	**bridge**	H: bridge[77]	−2.95	**−2.78**	**−2.83**	418, 903, 1382	0.17	14.0	295, 636, 974	0.12	20.6	**0.69**	**1.17**	**0.81**
	top		−2.87	−2.71	−2.75	295, 312, 2148	0.17	23.2	208, 220, 1514	0.12	29.7	0.67	1.22	1.08
Ni(100)	bridge	H[78] and D[79]: hollow	−2.69	−2.53	−2.57	163, 1163, 1321	0.16	20.4	115, 819, 931	0.12	26.9	0.72	1.20	0.86
	hollow		−2.77	**−2.66**	**−2.69**	524, 536, 728	0.11	19.2	369, 378, 513	0.08	27.0	**1.29**	**0.89**	**1.14**
Pd(100)	bridge	H[80] and D[81]: hollow	−2.76	−2.60	−2.64	202, 1213, 1232	0.16	19.3	143, 858, 871	0.12	25.2	0.73	1.21	0.88
	hollow		−2.75	**−2.69**	**−2.71**	70, 370, 546	0.06	40.3	49, 262, 386	0.04	48.5	**2.23**	**0.79**	**1.77**
Pt(100)	**bridge**	H: bridge+hollow[82]	−2.95	**−2.78**	**−2.83**	389, 1040, 1321	0.17	13.9	274, 733, 931	0.12	20.5	**0.67**	**1.19**	**0.79**
	top		−2.75	−2.58	−2.63	203, 212, 2245	0.17	29.3	143, 150, 1582	0.12	35.8	0.71	1.23	0.87
Cu(100)	bridge	H: hollow[83,84] D: hollow below 0.5ML[85]	−2.31	−2.15	−2.20	139, 1173, 1219	0.16	22.0	98, 827, 859	0.11	28.7	0.78	1.17	0.91
	hollow		−2.41	**−2.30**	**−2.33**	526, 538, 655	0.11	19.8	371, 379, 462	0.08	27.7	**1.35**	**0.88**	**1.18**
Ag(100)	bridge		−1.96	−1.82	−1.86	163, 1013, 1088	0.14	22.0	115, 714, 767	0.10	29.0	0.93	1.07	1.00
	hollow		−1.96	**−1.89**	**−1.91**	251, 322, 540	0.07	30.9	177, 228, 382	0.05	39.2	**2.05**	**0.80**	**1.64**
Au(100)	**bridge**		−2.22	**−2.06**	**−2.11**	355, 1059, 1137	0.16	15.2	250, 746, 801	0.11	22.0	**0.76**	**1.12**	**0.85**
	top		−1.92	−1.78	−1.82	140, 167, 2000	0.14	34.5	99, 118, 1414	0.10	41.1	0.91	1.17	1.07

[a] Calculated ν, ZPE, and S for gas phase H$_2$ and D$_2$ at 0.1 atm are 4314 cm^{-1}, 0.27 eV, 175.0 J/mol/K and 3041 cm^{-1}, 0.19 eV, 189.6 J/mol/K, respectively. [b] All entropies were calculated at 623 K. [c] Items in bold indicate the most stable sites on these surfaces.

The ZPE–corrected binding energies of H/D on the various (100) surfaces are in good agreement with the results reported in the literature.[61,67,77,86,87] On all surfaces, bridge and/or hollow sites are more favorable than top sites. On the (100) surfaces of Rh, Ni, Pd, and Ag, the hollow and bridge sites are almost isoenergetic; the difference in BEs are less than 0.1 eV.

Similar to the (111) surfaces, the most stable sites are the same for H and D. However, we note that for (100) surfaces, ZPE corrections are necessary to capture the binding site preferences of H/D in some cases. The ZPE corrections greatly destabilize binding on bridge and top sites, as compared to hollow sites. This is due to the narrower potential energy wells for H binding on top and bridge sites, which leads to higher vibrational frequencies for these sites compared to hollow sites. On Rh(100) and Pd(100) for example, bridge sites were more favorable without ZPE corrections. However, the hollow site was most preferred when the ZPE was taken into consideration. The preference for H to occupy hollow sites on these two metals is confirmed by experiments for both Pd(100)[80] and Rh(100).[75]

On the open (100) surfaces, we notice that bridge sites exhibit inverse TIEs, while normal TIEs larger than unity are found on the four–fold hollow sites. In fact, the calculated TIEs on hollow sites are larger than 1.1 for all of the considered open surfaces. This is because the ZPE contributions on hollow sites are much greater than unity and can be up to 3 times larger than that for bridge sites. In contrast, on the (111) surface (as well as the (211) surface, to be discussed in the next section), the ZPE contributions of most sites are less than unity. This interesting behavior can be explained as follows: as hollow sites have relatively softer vibrational modes compared to bridge sites, H and D end up having relatively similar ZPEs. The difference in gas phase H_2/D_2 ZPEs dominates, making H_2 dissociative adsorption thermodynamically more favorable as H_2 (g) is intrinsically less stable than D_2 (g) due to its larger ZPE.

C. TIEs on stepped fcc(211) surfaces

The step edges of metal nanoparticle catalysts may play a major role in H_2 dissociative adsorption, as H tends to bind more strongly on these under–coordinated sites. To examine the effect of steps on the TIEs of H_2/D_2 dissociative adsorption, we studied the fcc(211) surfaces of 8 transition metals. Fifteen different high symmetry adsorption sites were considered, as illustrated in **Figure 1(e)**. Summarized in **Table 3** are binding energies (B.E.), zero-point energy corrected binding energies (B.E. + ZPE), vibrational frequencies (ν), zero–point energies (ZPE), entropies (*S*), of H/D adsorption at low–coverage (θ = 1/9 ML), together with TIEs, including their breakdown into ZPE and entropic contributions, of H_2/D_2 dissociative adsorption on stepped fcc(211) surfaces.

Table 3 Calculated binding energies (B.E., eV), zero-point energy corrected binding energies (B.E. + ZPE$_H$ and B.E. + ZPE$_D$, eV), vibrational frequencies (ν, cm^{-1}), zero–point energies (ZPE, eV), and entropies (S, J/mol/K) for H/D adsorption, as well as ZPE contributions (TIE–ZPE), and entropic contributions (TIE–S) to the overall thermodynamic isotope effects (TIE–Overall) for H$_2$/D$_2$ dissociative adsorption at 623 K and a coverage of 1/9 ML on different stepped fcc(211) surfaces. Only stable sites are shown. Definitions of these terms can be found in the methods section.

Surface	Site	B.E.	B.E.+ZPE$_H$	B.E.+ZPE$_D$	H[a]			D[a]			TIE		
					ν_H	ZPE$_H$	S_H[b]	ν_D	ZPE$_D$	S_D[b]	ZPE	S	Overall
Rh(211)	hollow_a1	−2.81	−2.66	−2.70	502, 867, 1111	0.15	13.8	354, 611, 783	0.11	20.8	0.73	1.23	0.90
	hollow_a2[c]	−2.85	**−2.68**	**−2.73**	306, 1083, 1309	0.17	15.6	216, 763, 923	0.12	22.2	**0.64**	**1.37**	**0.88**
	hollow_b2	−2.74	−2.58	−2.63	704, 751, 1098	0.16	12.3	496, 529, 773	0.11	19.3	0.73	1.25	0.92
	hollow_c1	−2.75	−2.59	−2.64	672, 730, 1142	0.16	12.7	473, 514, 805	0.11	19.6	0.70	1.25	0.88
	hollow_c2	−2.73	−2.57	−2.62	724, 733, 1099	0.16	12.3	510, 517, 775	0.11	19.2	0.73	1.25	0.92
	top_b	−2.75	−2.59	−2.64	316, 926, 1356	0.16	16.1	223, 653, 956	0.11	22.8	0.70	1.32	0.92
Ir(211)	bridge_bc	−2.58	−2.43	−2.47	316, 604, 1481	0.15	18.5	223, 426, 1044	0.11	25.5	0.80	1.22	0.98
	hollow_a2	−3.06	**−2.89**	**−2.94**	432, 973, 1378	0.17	13.3	305, 686, 971	0.12	19.9	**0.59**	**1.38**	**0.81**
	hollow_b2	−2.55	−2.41	−2.45	496, 625, 1166	0.14	15.8	350, 441, 821	0.10	23.0	0.88	1.15	1.01
	hollow_c1	−2.57	−2.44	−2.48	299, 495, 1299	0.13	20.9	211, 349, 915	0.09	28.2	1.00	1.11	1.11
	hollow_c2	−2.57	−2.43	−2.47	451, 583, 1187	0.14	16.9	318, 411, 836	0.10	24.2	0.92	1.13	1.04
	top_a	−2.90	−2.73	−2.78	257, 312, 2124	0.17	24.3	181, 220, 1497	0.12	30.8	0.64	1.31	0.84
	top_b	−2.87	−2.70	−2.75	466, 842, 1433	0.17	13.4	328, 594, 1010	0.12	20.1	0.61	1.35	0.83
	top_c	−2.66	−2.47	−2.53	403, 443, 2156	0.19	18.0	284, 312, 1520	0.13	24.3	0.49	1.40	0.83
Ni(211)	bridge_a	−2.76	−2.59	−2.64	128, 1227, 1313	0.17	22.1	90, 865, 925	0.12	28.6	0.67	1.41	0.95
	hollow_a1	−2.84	**−2.67**	**−2.72**	719, 926, 1159	0.17	10.6	507, 653, 817	0.12	17.3	**0.59**	**1.37**	**0.81**
	hollow_b1	−2.69	−2.58	−2.61	452, 593, 759	0.11	19.3	318, 418, 535	0.08	27.1	1.31	0.97	1.27
	hollow_b2	−2.74	−2.57	−2.62	802, 888, 1122	0.17	10.3	566, 626, 791	0.12	17.0	0.59	1.37	0.81
	hollow_c1	−2.77	−2.59	−2.64	858, 859, 1160	0.18	10.0	604, 605, 818	0.13	16.5	0.56	1.41	0.79
	hollow_c2	−2.78	−2.61	−2.66	819, 831, 1162	0.17	10.4	577, 586, 819	0.12	17.1	0.59	1.37	0.81
	top_b	−2.61	−2.45	−2.50	176, 1081, 1346	0.16	20.0	124, 762, 948	0.11	26.6	0.70	1.36	0.95
Pd(211)	**hollow_a1**	−2.80	−2.64	**−2.69**	719, 926, 951	0.16	11.7	506, 652, 670	0.11	18.6	**0.67**	**1.27**	**0.85**
	hollow_a2	−2.76	−2.59	−2.64	240, 1206, 1281	0.17	17.2	169, 850, 903	0.12	23.7	0.61	1.40	0.86
	hollow_b2	−2.81	**−2.65**	**−2.69**	781, 874, 988	0.16	11.3	551, 616, 696	0.12	18.1	**0.64**	**1.29**	**0.83**

	Site				Frequencies	ZPE	S	Frequencies	ZPE	S			
	hollow_c1	−2.81	**−2.65**	**−2.69**	821, 830, 983	0.16	11.3	579, 585, 693	0.12	18.2	**0.67**	**1.29**	**0.86**
	hollow_c2	−2.79	−2.63	−2.68	807, 834, 959	0.16	11.5	569, 588, 676	0.11	18.4	0.70	1.27	0.89
	top_b	−2.66	−2.50	−2.54	214, 1168, 1255	0.16	18.3	151, 823, 885	0.12	24.9	0.64	1.37	0.88
Pt(211)	**bridge_a**	−2.90	**−2.73**	**−2.78**	382, 1048, 1309	0.17	14.1	269, 739, 922	0.12	20.7	**0.61**	**1.37**	**0.84**
	bridge_bc	−2.63	−2.47	−2.52	309, 894, 1406	0.16	16.3	218, 630, 991	0.11	23.0	0.67	1.32	0.89
	bridge_ca	−2.67	−2.52	−2.56	245, 802, 1362	0.15	19.0	173, 565, 960	0.11	25.9	0.80	1.24	1.00
	hollow_b2	−2.62	−2.48	−2.52	458, 656, 1178	0.14	16.0	322, 462, 830	0.10	23.2	0.88	1.16	1.01
	hollow_c1	−2.63	−2.50	−2.53	432, 596, 1138	0.13	17.3	305, 420, 802	0.10	24.6	1.00	1.11	1.11
	hollow_c2	−2.66	−2.52	−2.56	508, 561, 1106	0.14	16.6	358, 396, 779	0.10	23.9	0.96	1.11	1.06
	top_a	−2.76	−2.58	−2.64	294, 331, 2206	0.18	22.7	207, 234, 1554	0.12	29.2	0.59	1.35	1.39
	top_b	−2.74	−2.57	−2.62	409, 1004, 1380	0.17	13.5	288, 707, 973	0.12	20.1	0.59	1.39	0.82
	top_c	−2.72	−2.53	−2.59	377, 393, 2269	0.19	19.4	266, 277, 1599	0.13	25.7	0.49	1.40	0.69
Cu(211)	**hollow_a1**	−2.55	**−2.38**	**−2.43**	669, 920, 1096	0.17	11.4	471, 648, 772	0.12	18.2	**0.64**	**1.31**	**0.84**
	hollow_b1	−2.30	−2.19	−2.22	416, 632, 711	0.11	19.9	293, 445, 501	0.08	27.7	1.36	0.96	1.31
	hollow_b2	−2.38	−2.21	−2.26	790, 896, 1035	0.17	10.8	557, 631, 730	0.12	17.5	0.61	1.33	0.82
	hollow_c1	−2.43	−2.26	−2.31	840, 898, 1053	0.17	10.3	592, 633, 742	0.12	17.0	0.59	1.36	0.80
	hollow_c2	−2.47	−2.30	−2.35	797, 814, 1086	0.17	11.1	562, 573, 765	0.12	17.9	0.64	1.32	0.85
	top_b	−2.20	−2.05	−2.09	111, 1101, 1232	0.15	24.1	78, 776, 868	0.11	30.9	0.77	1.31	1.00
Ag(211)	**hollow_a1**	−2.13	**−1.99**	**−2.03**	526, 807, 885	0.14	15.1	371, 569, 624	0.10	22.4	**0.92**	**1.12**	**1.02**
	hollow_b2	−2.02	−1.88	−1.92	703, 759, 852	0.14	13.7	495, 535, 600	0.10	20.9	0.88	1.15	1.00
	hollow_c1	−2.06	−1.91	−1.96	727, 782, 835	0.15	13.4	512, 551, 589	0.10	20.6	0.84	1.16	0.97
	hollow_c2	−2.07	−1.93	−1.97	668, 712, 852	0.14	14.5	471, 502, 601	0.10	21.8	0.96	1.11	1.07
	top_b	−1.89	−1.75	−1.79	144, 1025, 1050	0.14	23.1	102, 722, 740	0.10	30.1	0.92	1.19	1.09
Au(211)	**bridge_a**	−2.30	**−2.14**	**−2.19**	329, 1094, 1114	0.16	15.7	232, 771, 785	0.11	22.5	**0.73**	**1.29**	**0.94**
	hollow_b2	−2.02	−1.88	−1.92	639, 715, 935	0.14	14.2	450, 504, 659	0.10	21.4	0.88	1.14	1.00
	hollow_c1	−2.06	−1.92	−1.96	555, 777, 880	0.14	15.0	391, 548, 620	0.10	22.3	0.96	1.11	1.06
	hollow_c2	−2.12	−1.99	−2.03	592, 652, 879	0.13	15.7	417, 459, 619	0.09	23.2	1.00	1.08	1.08
	top_a	−2.02	−1.87	−1.91	195, 255, 2015	0.15	28.3	137, 179, 1420	0.11	35.0	0.77	1.26	0.97
	top_b	−2.11	−1.95	−2.00	345, 1043, 1191	0.16	15.3	243, 735, 840	0.11	22.1	0.70	1.30	0.91
	top_c	−1.86	−1.71	−1.75	200, 217, 1985	0.15	29.4	141, 153, 1399	0.11	36.1	0.80	1.25	1.00

[a] Calculated ν, ZPE, and S for gas phase H_2 and D_2 at 0.1 atm are 4314 cm^{-1}, 0.27 eV, 175.0 J/mol/K and 3041 cm^{-1}, 0.19 eV, 189.6 J/mol/K, respectively. [b] All entropies were calculated at 623 K. [c] Items in bold indicate the most stable sites on these surfaces.

On the stepped surfaces studied, the binding energy of H ranges from −3.06 eV (hollow_a2 site of Ir(211)) to −1.86 eV (top_c site of Au(211)). Our results are in good agreement with previous DFT studies.[88–90] On Pt(211) and Au(211), bridge_a, which lies on the step edge, is the most stable adsorption site, while on other (211) metal surfaces studied, hollow sites near the step edge are most energetically favorable. Similar to the (100) surfaces, top sites are the least favorable sites on all of the studied (211) surfaces.

Similar to the (111) and (100) surfaces, we do not predict any change in the preferred binding sites upon switching H for D, except in the case of Pd(211), where the hollow_a1 site, which was originally 0.01 eV less favorable than the hollow_b2 and hollow_c1 sites for H, becomes isoenergetic with them in the case of D. This energy difference is however well within the error of our calculations.

The TIEs on the stepped (211) surfaces are in a similar range as those on close–packed surfaces, varying from 0.70 on the top_c site on Ir(211), to 1.15 on the hollow_b1 site on Cu(211). In terms of the entropic and ZPE contributions to the TIEs, the (211) surfaces are also very similar to the (111) surfaces, with ZPE contributions mostly smaller than unity, and entropic contributions mostly larger than unity.

A comparison of results on all three surface types reveals some interesting observations regarding the structure sensitivity of the reaction energetics, as well as of the TIEs. On Rh and Ni, the B.E.s of H on the three different surfaces studied are all very similar, indicating that dissociative adsorption of H_2 is probably insensitive to the surface structure of Rh and Ni, in agreement with existing literature.[73,89] In contrast, the B.E. of H on Ir(211) is about 0.3 eV higher in magnitude than that on Ir(111). Pt(100), Ag(211), and Au(211) also bind H stronger by 0.1 −

0.2 eV compared to Pt(111), Ag(100), and Au(111). Judging from these thermodynamics alone, dissociative adsorption of H_2 on Ir, Pt, Ag, and Au, is probably structure sensitive. In fact, we confirm that H_2 dissociative adsorption on Au is structure sensitive in the next section where we have calculated the transition states for this reaction.

Interestingly, the TIE values for the most stable sites on the (111) and (211) surfaces are all below unity. However, on the (100) surfaces, the most stable sites, which are commonly hollow sites, exhibit TIEs greater than unity. For example, the calculated TIEs on Ni(111), (100), and (211) surfaces are 0.71, 1.11, and 0.75, respectively. This finding opens up the possibility of utilizing TIEs for determination of the dominant facets, whether close–packed or open, of transition metal nanoparticle catalysts. For example, if a normal TIE (> 1) is measured for H_2 dissociative adsorption on a catalyst of unknown morphology, we can draw several preliminary conclusions. Firstly, it is likely that there is a significant proportion of (100) facets. Secondly, H is bound on the hollow sites of these (100) facets. Lastly, if diffusion is not facile, we might also conclude that dissociative adsorption occurs on the (100) facets (as opposed to on other facets, with the H eventually diffusing to and adsorbing on the hollow sites). However, in order to determine conclusively if the dissociation event actually occurs on the (100) facets, KIE measurements would be necessary.

This would not work well for metals which do not bind H on (100) hollow sites i.e. on Ir, Pt, and Au. On these metals, the TIEs of the most stable sites on different surfaces are very close to each other. For example, on Ir(111), (100), and (211) surfaces, the calculated TIEs are 0.70, 0.78 and 0.76, respectively.

D. KIEs on noble metal (Cu, Ag and Au) surfaces

In addition to the TIEs, we have also studied the kinetic isotope effects (KIEs) for H_2/D_2 dissociative adsorption on three different surfaces of three noble metals, Cu, Ag, and Au, on which the dissociation process has been found to be highly activated.[91,92] **Figure 2** shows the transition state (TS) geometries, while **Table 4** summarizes the activation energy barriers (E_a), zero-point energy corrected activation barriers (E_a + ZPE), TS frequencies (ν), zero–point energies (ZPE), entropies (S), and the calculated KIEs, including their breakdown into ZPE and entropic contributions, on the surfaces of the three metals considered.
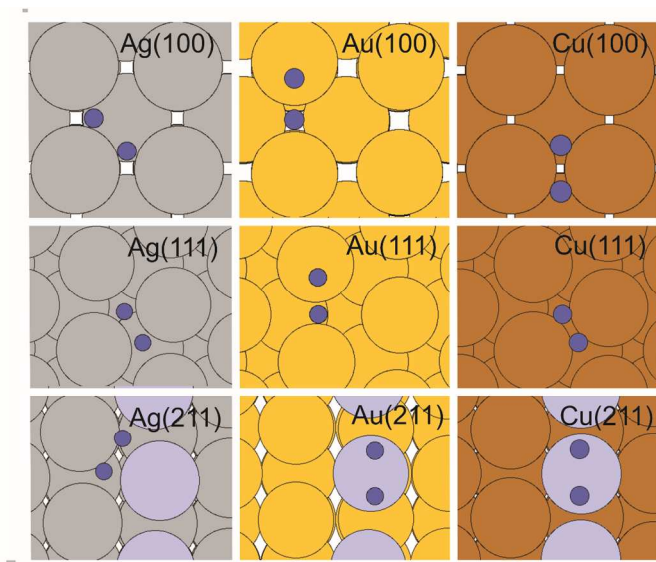
Figure 2. Top view of transition state geometries for H_2/D_2 dissociative adsorption on Ag, Au, and Cu surfaces. Color code: H/D – blue, Ag – silver, Au – yellow, Cu – brown, step edge atoms – light purple.

Table 4 Calculated activation energy barriers (E_a, eV), zero-point energy corrected activation barriers ($E_a + ZPE_{TS} - ZPE_{IS}$, eV), vibrational frequencies (v, cm^{-1}), zero–point energies (ZPE, eV), entropies (S, J/mol/K) of transition states, as well as ZPE contributions (KIE–ZPE) and entropic contributions (KIE–S) to the overall kinetic isotope effect (KIE–Overall) for H_2/D_2 dissociative adsorption at 623 K on various noble metal surfaces. Definitions of these terms can be found in the methods section.

surface	Expt.		Calc			H[a]			D[a]			KIE		
	$E_{a,H2}$	$E_{a,D2}$	E_a[c]	$E_a +$ ZPE_{H-TS} $- ZPE_{H2}$	$E_a +$ ZPE_{D-TS} $- ZPE_{D2}$	$v_{H–TS}$	$ZPE_{H–TS}$	$S_{H–TS}$[b]	$v_{D–TS}$	$ZPE_{D–TS}$	$S_{D–TS}$[b]	ZPE	S	Overall
Cu(111)	~0.6[93,94] 0.54[95]	0.60[96]	0.48	0.47	0.46	500i, 345, 385, 767, 968, 1655	0.26	28.6	353i, 244, 272, 542, 684, 1170	0.18	40.0	1.06	1.48	1.57
Ag(111)		>0.8[92]	1.09	1.03	1.05	1230i, 354, 556, 724, 822, 847	0.21	30.0	870i, 250, 393, 512, 581, 599	0.15	42.5	1.40	1.29	1.81
Au(111)			0.97	0.95	0.96	853i, 209, 407, 595, 928, 1789	0.25	31.3	603i, 207,287, 420,656, 1265	0.18	42.7	1.10	1.46	1.61
Cu(100)	0.50[97]	0.58[97]	0.56	0.54	0.55	1028i, 440, 630, 874, 990, 1133	0.25	23.6	727i, 311,446, 618, 700, 801	0.18	35.2	1.08	1.44	1.55
Ag(100)			1.10	1.06	1.07	952i, 616, 626, 716, 792, 974	0.23	24.5	673i, 434, 443, 507, 560, 688	0.16	36.6	1.21	1.36	1.65
Au(100)			0.69	0.68	0.68	676i, 320, 449, 679, 920, 1808	0.26	28.9	478i, 226, 318, 480, 650, 1278	0.18	40.2	1.04	1.48	1.54
Cu(211)			0.54	0.56	0.56	1230i, 241, 546, 659, 1604, 1647	0.29	27.7	870i, 170, 386, 466, 1134, 1165	0.21	38.3	0.87	1.61	1.41
Ag(211)			1.10	1.03	1.05	1222i, 403, 521, 664, 779, 855	0.20	30.4	864i, 285, 368, 469, 550, 604	0.14	42.9	1.44	1.28	1.84
Au(211)			0.71	0.75	0.74	901i, 291, 321, 789, 1693, 1909	0.31	28.6	637i, 205, 226, 558, 1197, 1350	0.22	38.8	0.79	1.69	1.33

[a] Calculated v, ZPE, and S for gas phase H_2 and D_2 at 0.1 atm and 623 K are 4314 cm^{-1}, 0.27 eV, 175.0 J/mol/K and 3041 cm^{-1}, 0.19 eV, 189.6 J/mol/K, respectively. [b] Entropies were calculated at 623 K. [c] E_a is reported with respect to H_2 (g) / D_2 (g).

The dissociation barriers are observed to decrease in the order of Ag > Au > Cu, for all of the facets studied. Our calculated activation energy barriers on close–packed and open surfaces are consistent with earlier theoretical studies.[98–102] There is also good agreement with experimentally obtained activation energies. Due to the ZPE differences largely cancelling out, there is little difference (maximum 0.02 eV) in the ZPE corrected activation energies between H_2 and D_2 dissociative adsorption, and thus the active sites for H_2/D_2 dissociative adsorption are expected to be the same.

On all surfaces of Cu, Ag, and Au, normal KIEs (> 1) are observed, indicating that the reaction rate constants for dissociation of H_2 (g) are larger than that of D_2 (g) under the studied conditions. Decomposing the KIE into its entropic and ZPE components, we note that the entropic contributions are much larger than unity for all surfaces. This is attributed to reasons similar to those noted for the TIEs on the (111) and (211) surfaces, namely the smaller difference in entropies in the TS (in the case of the TIEs, the final state (FS)) as compared to the gas phase.

Except for Cu(211) and Au(211), the ZPE contributions are also larger than unity. This is a classic primary KIE: as the ZPE differences between the TSs are smaller compared to the ZPE differences between the ISs, the ZPE–corrected activation energies for H_2 (g) are lower than those for D_2 (g). On Cu(211) and Au(211), we trace the inverse ZPE contributions back to stiff vibrational modes (~1600–1900 cm^{-1}) perpendicular to the surface, which gives rise to a larger ZPE difference in the TS compared to the IS.

We now compare the structure sensitivity of H_2/D_2 dissociative adsorption *in terms of reaction rates*, versus the structure sensitivity of the reaction *in terms of KIEs*. On Ag, this reaction might traditionally be considered structure insensitive because there is essentially no difference in E_a

for all three surfaces; see Table 4. The KIEs however, do exhibit structure sensitivity; the KIEs on Ag(111), Ag(100) and Ag(211) are 1.81, 1.65, and 1.84 respectively. The large difference in KIEs between Ag(100) the other two Ag surfaces, even though activation energies (for dissociation of the same isotope) on different surfaces do not differ appreciably, suggests that on Ag, KIEs might offer a viable means of determining active sites for the dissociative adsorption of H_2/D_2.

On Cu, H_2/D_2 dissociative adsorption might also be structure insensitive since the reaction barriers on all three Cu surfaces are similar to within 0.1 eV. KIE values on Cu surfaces have the narrowest range out of the three metals considered, varying from 1.41 (for Cu(211)) to 1.57 (for Cu(111)), indicating that isotope exchange effects are the least structure sensitive on Cu.

For Au, H_2/D_2 dissociative adsorption is structure sensitive; the activation energy barrier is 0.97 eV on the close-packed Au(111) surface and ~0.7 eV on Au(100) and Au(211). The largest range of KIEs among the three surfaces of the same metal is found here; the KIE is smallest (1.33) on Au(211), and largest (1.61) on Au(111). This is due to a much smaller ZPE contribution on Au(211) than that on Au(100) and Au(111).

Based on the above analysis, it is clear that the structure sensitivity of H_2/D_2 dissociative adsorption may differ depending on whether one evaluates the structure sensitivity in terms of reaction rates, or instead in terms of KIEs. Isotope effects may thus be a useful complementary tool for probing and identifying the catalytically active sites of transition metal nanoparticles even when reactions are structure insensitive in terms of rates for a single isotope.

E. Temperature dependence of TIE and KIE

Finally, we have investigated the temperature dependence of the TIEs and KIEs for H_2/D_2 dissociative adsorption. **Figures 3 – 5** show Arrhenius plots for TIEs with H binding on the most stable sites of the studied close–packed, open, and stepped surfaces of transition metals, respectively, as the temperature is varied from 523 K to 673 K. For Arrhenius plots of TIEs with H binding on the less stable sites, the reader is referred to **Figures S1-3** for the close–packed surfaces, **Figures S4-6** for the open surfaces, and **Figures S7-16** for the stepped surfaces. **Figure 6** shows the Arrhenius plot for the KIEs on different surfaces of the 3 noble metals, for the same temperature range.
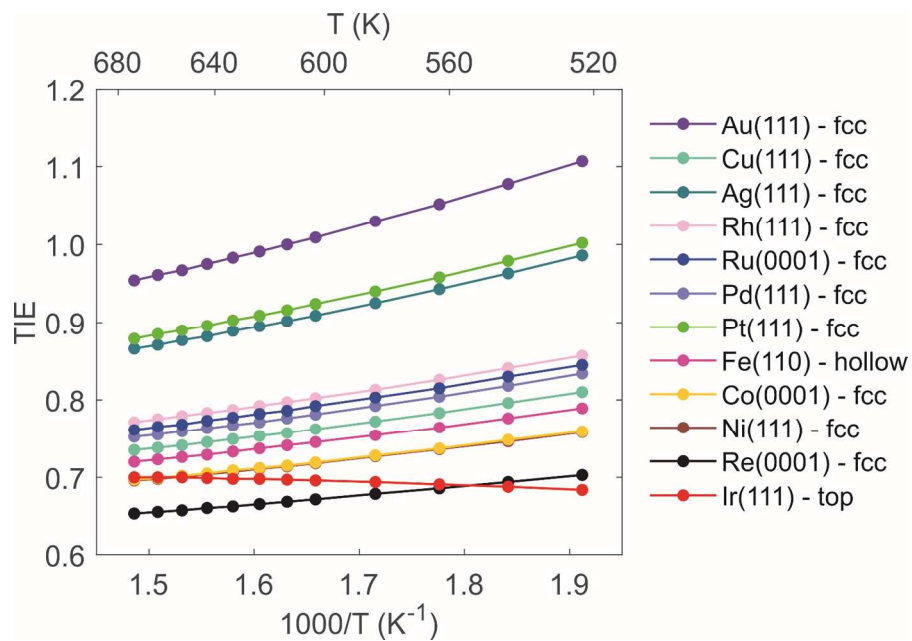
Figure 3. Arrhenius plots for the thermodynamic isotope effects of H$_2$ and D$_2$ dissociative adsorption on the most stable site (see legend) of each close–packed transition metal surface. Ni(111) – fcc line is partially covered by the Co(0001) – fcc line.
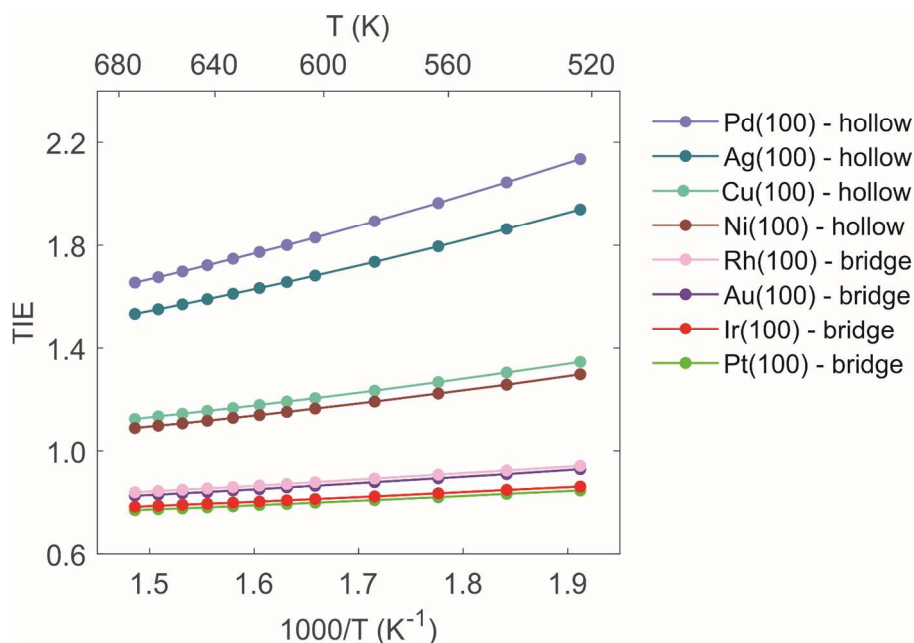
Figure 4. Arrhenius plots for the thermodynamic isotope effects of H$_2$ and D$_2$ dissociative adsorption on the most stable site (see legend) of the fcc(100) surfaces of transition metals.
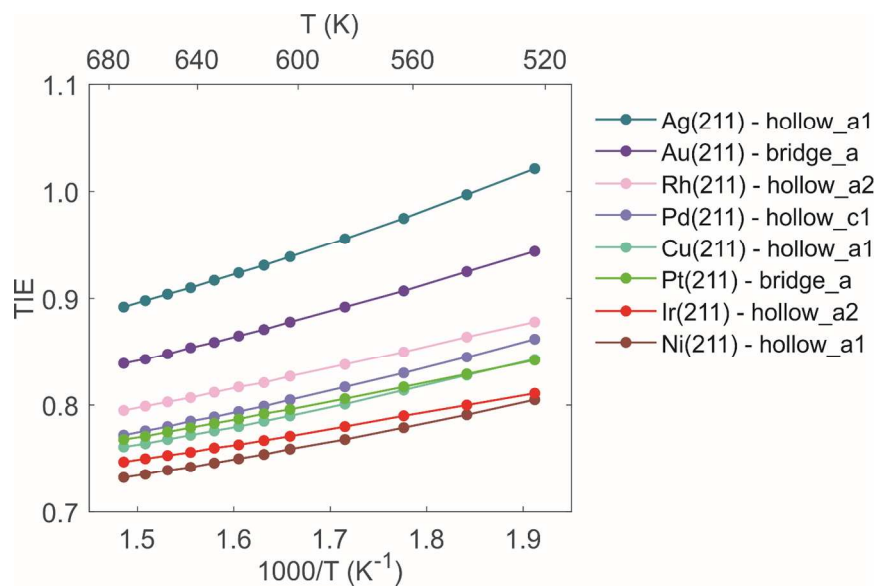
Figure 5. Arrhenius plots for the thermodynamic isotope effects of H_2 and D_2 dissociative adsorption on the most stable sites (see legend) of the fcc(211) surfaces of transition metals.

The slope of the Arrhenius plots varies for different sites due to the varying ZPE and entropic contributions, and the effect of temperature on each of these quantities.

From equations (6) and (7), the ZPE contribution decreases with decreasing temperature as it is proportional to $\exp(-\frac{1}{T})$, and there is no temperature dependence in the $\left(ZPE_H^{FS} - ZPE_H^{IS}\right) - \left(ZPE_D^{FS} - ZPE_D^{IS}\right)$ term.

The entropic contribution however, as shown in equation (2), increases with decreasing temperature due to the increase in the entropy difference $\left(S_H^{FS} - S_H^{IS}\right) - \left(S_D^{FS} - S_D^{IS}\right)$ as temperature decreases. We can rearrange this difference in terms of an initial state contribution and a final state contribution i.e. $\left(S_D^{IS} - S_H^{IS}\right) + \left(S_H^{FS} - S_D^{FS}\right)$. The difference in entropy of the initial states, H_2 (g) and D_2 (g), which is encompassed in the $\left(S_D^{IS} - S_H^{IS}\right)$ term, is positive. It has a weak dependence on temperature due to the large H_2 and D_2 vibrational frequencies of 4314 and 3041 cm^{-1} respectively. Thus, trends in the entropy contribution are dominated by differences in the entropy of the final states i.e. adsorbed H/D, which is the $\left(S_H^{FS} - S_D^{FS}\right)$ term. This term grows less negative with decreasing temperature due to the large decrease in vibrational entropy of adsorbed D thus leading to an increase in the entropy contribution with decreasing temperature.

Of the two contributions, the entropic contribution is found to be dominant for both TIEs and KIEs, leading to an observed overall increase in TIEs and KIEs with decreasing temperature. For example, for the Pt(111) fcc site, the ZPE contribution to the TIE decreases from 0.90 at 673 K to 0.87 at 523 K (~3 % decrease), while the entropic contribution increases from 0.98 to 1.15 (~17 % increase).

A notable exception is the top site of Pt(111) (and also the top site of Ir(111), see **Figure S1**) which the TIE decrease with decreasing temperature. This is because the small ZPE contributions (~0.5–0.6) to the TIEs on these sites increase relatively rapidly with increasing temperature compared the ZPE contributions of other sites. This allows the ZPE contributions to dominate the trend for these two top sites.

Additionally, we observe that the differences in TIEs among the different site types grow larger as temperature decreases. From example, on Ag(211), the difference in the TIEs of different site types increases from ~0.15 at high temperatures to ~0.25 at lower temperatures. Measurements of TIEs that are done at lower temperatures could thus be more effective at differentiating between different site types, although caution should be taken to ensure that the system is not kinetically trapped at these lower temperatures (i.e. the most thermodymically favorable sites are not kinetically accessible).

The same trend of increasing KIE difference with lower temperatures is also observed for the different noble metal surfaces. To identify the most active site for the reaction, KIEs should thus be ideally measured at lower temperatures, since in this way contributions from other less active sites are minimized, while the KIE difference is maximized.
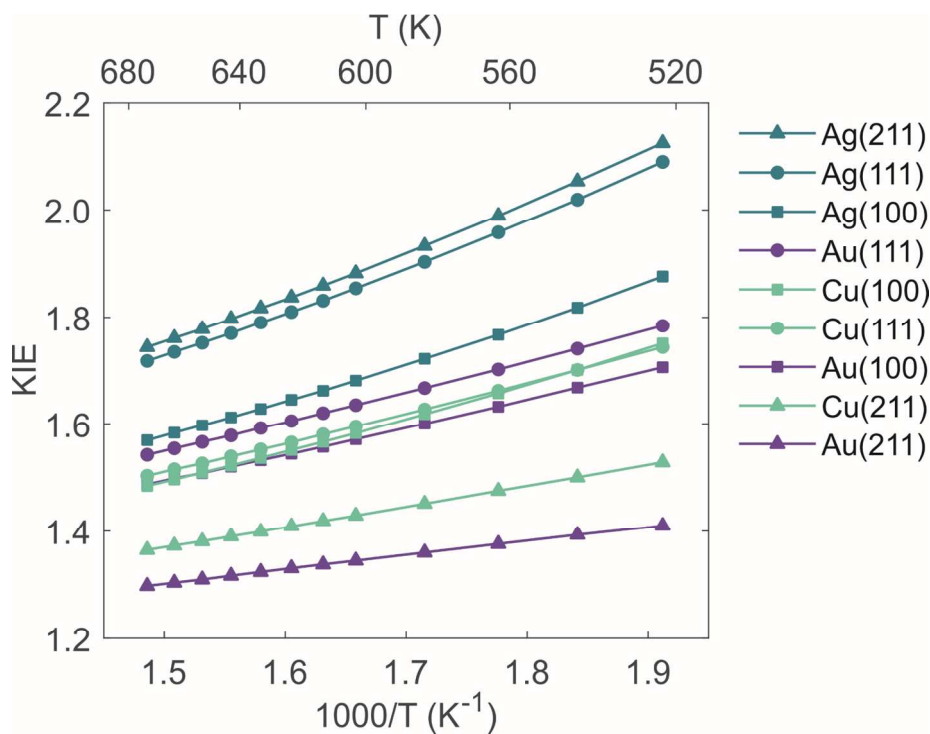
Figure 6. Arrhenius plots for the kinetic isotope effects of H_2/D_2 dissociative adsorption on various surfaces of Cu, Ag, and Au as a function of temperature (T).

4. Conclusions

In summary, using planewave DFT-based calculations, we have systematically studied H_2/D_2 dissociative adsorption on 28 surfaces of 12 different transition metals at the low coverage limit (1/9 ML). We note that one must also consider the relevant coverages involved in a reaction system when making direct comparisons with our calculated values; higher coverages of H under realistic reaction conditions may result in shifts in the TIEs and KIEs. Bearing this in mind, the calculated TIEs and KIEs can be very useful for probing reaction mechanisms involving hydrogen bond–making/breaking.

We showed that TIEs may be used to determine the site preference of H_2 dissociative adsorption by helping us discriminate between two energetically competitive sites. On close–packed as well as fcc(211) surfaces, sites with TIEs larger than unity were not the most preferred sites for H/D binding. Most of these favorable sites have TIE values of ~0.70–0.80. However, on fcc(100) surfaces, the four–fold hollow sites, which are often the most preferred binding sites, all have TIEs larger than unity. These large differences in TIEs between the most stable sites of various surface structures can thus be used as a tool, complementary to other experimental and computational approaches, in order to characterize transition metal catalysts and elucidate the dominant facets and site types present on them.

Furthermore, KIEs can therefore be used to identify the active sites for H_2/D_2 dissociative adsorption on different transition metal surfaces. In terms of activation energies, H_2 dissociation is structure sensitive on Au, while it is structure insensitive on Cu and Ag. However, for all three metals, there are notable differences in the KIEs for different surfaces, indicating that the reaction is structure sensitive in terms of its KIEs.

Lastly, the temperature dependence of TIEs and KIEs was analyzed and was found to increase with decreasing temperature for most site types and surfaces considered, showing that experimental measurements of TIEs and KIEs should be done at low temperatures to maximize the signal-to-noise ratio of the measurements.

Our study provides a systematic DFT database on TIEs and KIEs for H_2/D_2 dissociative adsorption on various transition metal surfaces, which we hope will spur on further research into the multitude of uses that TIEs and KIEs possess.

Conflicts of Interest

There are no conflicts to declare.

Acknowledgements

References

1   M. Ojeda, A. Li, R. Nabar, A. U. Nilekar, M. Mavrikakis and E. Iglesia, *J. Phys. Chem. C*, 2010, **114**, 19761–19770.
2   R. A. Dallabetta and M. Shelef, *J. Catal.*, 1977, **49**, 383–385.
3   M. Shelef and R. A. Dallabatta, *J. Catal.*, 1979, **60**, 169–170.
4   T. P. Wilson, *J. Catal.*, 1979, **60**, 167–168.
5   S. Krishnamoorthy, M. Tu, M. P. Ojeda, D. Pinna and E. Iglesia, *J. Catal.*, 2002, **211**, 422–433.
6   J. M. Wei and E. Iglesia, *Phys. Chem. Chem. Phys.*, 2004, **6**, 3754–3759.
7   T. Herranz, X. Y. Deng, A. Cabot, J. G. Guo and M. Salmeron, *J. Phys. Chem. B*, 2009, **113**, 10721–10727.
8   C. Kemball, *J. Chem. Soc.*, 1956, 735.
9   S. A. Goddard, R. D. Cortright and J. A. Dumesic, *J. Catal.*, 1992, **137**, 186–198.
10   E. M. Simmons and J. F. Hartwig, *Angew. Chemie Int. Ed.*, 2012, **51**, 3066–3072.
11   I. Houriuti and M. Polanyi, *J. Chem. Soc. Faraday Trans.*, 1934, **30**, 1164–1172.
12   H. M. Wang and E. Iglesia, *J. Catal.*, 2010, **273**, 245–256.
13   M. L. Burke and R. J. Madix, *J. Am. Chem. Soc.*, 1991, **113**, 4151–4157.
14   K. Yokozaki, H. Ono and A. Ayame, *Appl. Catal. A-General*, 2008, **335**, 121–136.
15   J. S. M. Samec, J. E. Backvall, P. G. Andersson and P. Brandt, *Chem. Soc. Rev.*, 2006, **35**, 237–248.
16   J. Atzrodt, V. Derdau, T. Fey and J. Zimmermann, *Angew. Chemie Int. Ed.*, 2007, **46**, 7744–7765.
17   M. Montano, K. Bratlie, M. Salmeron and G. A. Somorjai, *J. Am. Chem. Soc.*, 2006, **128**, 13229–13234.
18   J.-H. Wang and C.-M. Chiang, *J. Am. Chem. Soc.*, 2000, **122**, 11521–11522.
19   G. Kresse and J. Furthmüller, *Comput. Mater. Sci.*, 1996, **6**, 15–50.
20   G. Kresse and J. Furthmüller, *Phys. Rev. B*, 1996, **54**, 11169–11186.
21   P. E. Blochl, *Phys. Rev. B*, 1994, **50**, 17953–17979.

22   G. Kresse and D. Joubert, *Phys. Rev. B*, 1999, **59**, 1758–1775.

23   J. P. Perdew and Y. Wang, *Phys. Rev. B*, 1992, **45**, 13244–13249.

24   S. Grimme, J. Antony, S. Ehrlich and H. Krieg, *J. Chem. Phys.*, 2010, **132**, 154104.

25   J. Klimeš, D. R. Bowler and A. Michaelides, *Phys. Rev. B*, 2011, **83**, 195131.

26   T. Thonhauser, V. R. Cooper, S. Li, A. Puzder, P. Hyldgaard and D. C. Langreth, *Phys. Rev. B*, 2007, **76**, 125112.

27   P. Janthon, S. M. Kozlov, F. Viñes, J. Limtrakul and F. Illas, *J. Chem. Theory Comput.*, 2013, **9**, 1631–1640.

28   L. Vega, J. Ruvireta, F. Viñes and F. Illas, *J. Chem. Theory Comput.*, 2018, **14**, 395–403.

29   P. Janthon, S. (Andy) Luo, S. M. Kozlov, F. Viñes, J. Limtrakul, D. G. Truhlar and F. Illas, *J. Chem. Theory Comput.*, 2014, **10**, 3832–3839.

30   H. J. Monkhorst and J. D. Pack, *Phys. Rev. B*, 1976, **13**, 5188–5192.

31   L. Bengtsson, *Phys. Rev. B*, 1999, **59**, 12301–12304.

32   J. Neugebauer and M. Scheffler, *Phys. Rev. B*, 1992, **46**, 16067–16080.

33   G. Henkelman, B. P. Uberuaga and H. Jonsson, *J. Chem. Phys.*, 2000, **113**, 9901–9904.

34   M. Nishijima, H. Okuyama, N. Takagi, T. Aruga and W. Brenig, *Surf. Sci. Rep.*, 2005, **57**, 113–156.

35   R. J. Behm, K. Christmann, G. Ertl, M. A. Van Hove and W. H. Weinberg, *Surf. Sci.*, 1979, **70**, 4168–4184.

36   C. M. Mate and G. A. Somorjai, *Phys. Rev. B*, 1986, **34**, 7417–7420.

37   M. Jørgensen and H. Grönbeck, *J. Phys. Chem. C*, 2017, **121**, 7199–7207.

38   L. H. Sprowl, C. T. Campbell and L. Árnadóttir, *J. Phys. Chem. C*, 2016, **120**, 9719–9731.

39   G. Kyriakou, E. R. M. Davidson, G. Peng, L. T. Roling, S. Singh, M. B. Boucher, M. D. Marcinkowski, M. Mavrikakis, A. Michaelides and E. C. H. Sykes, *ACS Nano*, 2014, **8**, 4827–4835.

40   J. Kästner, *Wiley Interdiscip. Rev. Comput. Mol. Sci.*, 2014, **4**, 158–168.

41   W. H. Miller, *Acc. Chem. Res.*, 1993, **26**, 174–181.

42   D. E. Jiang and E. A. Carter, *Surf. Sci.*, 2003, **547**, 95–98.

43   L. Hammer, H. Landskron, W. Nichtl-Pecher, A. Fricke, K. Heinz and K. Müller, *Phys. Rev. B*, 1993, **47**, 15969–15972.

44   K. L. Kostov, W. Widdra and D. Menzel, *Surf. Sci.*, 2004, **560**, 130–144.

45   M. Lindroos, H. Pfnür, P. Feulner and D. Menzel, *Surf. Sci.*, 1987, **180**, 237–251.

46   H. Conrad, R. Scala, W. Stenzel and R. Unwin, *J Chem Phys*, 1984, **81**, 6371–6378.

47   Z. Huesges and K. Christmann, *Zeitschrift für Phys. Chemie*, 2013, **227**, 881–899.

48   H. Yanagita, H. Fujioka, T. Aruga, N. Takagi and M. Nishijima, *Surf. Sci.*, 1999, **441**, 507–514.

49   M. Fukuoka, M. Okada, M. Matsumoto, S. Ogura, K. Fukutani and T. Kasai, *Phys. Rev. B*, 2007, **75**, 235434.

50   C. J. Hagedorn, M. J. Weiss and W. H. Weinberg, *Phys. Rev. B*, 1999, **60**, R14016–R14018.

51   E. Sailer; and C. Varelas, *Nucl. Instruments Methods Phys. Res. B2*, 1984, **2**, 326–329.

52   H. Okuyama, T. Ueda, T. Aruga and M. Nishijima, *Phys. Rev. B*, 2001, **63**, 233403.

53   T. E. Felter, E. C. Sowa and M. A. Van Hove, *Phys. Rev. B*, 1989, **40**, 891–899.

54   O. Løvvik and R. Olsen, *Phys. Rev. B*, 1998, **58**, 10890–10898.

55   C. H. Hsu, B. E. Larson, M. El-Batanouny, C. R. Willis and K. M. Martini, *Phys. Rev. Lett.*, 1991, **66**, 3164–3167.

56   K. M. Lui, Y. Kim, W. M. Lau and J. W. Rabalais, *Appl. Phys. Lett.*, 1999, **75**, 587–589.

57   K. Mortensen, C. Klink, F. Jensen, F. Besenbacher and I. Stensgaard, *Surf. Sci.*, 1989, **211/212**, 813–818.

58   S. C. Badescu, P. Salo, T. Ala-Nissila, S. C. Ying, K. Jacobi, Y. Wang, K. Bedurftig and G. Ertl, *Phys. Rev. Lett.*, 2001, **88**, 136101.

59   G. Lee and E. . Plummer, *Surf. Sci.*, 2002, **498**, 229–236.

60   G. Lee and E. W. Plummer, *Phys. Rev. B*, 1995, **51**, 7250–7261.

61   P. Ferrin, S. Kandoi, A. U. Nilekar and M. Mavrikakis, *Surf. Sci.*, 2012, **606**, 679–689.

62   V. Pallassana, M. Neurock, L. Hansen, B. Hammer and J. Nørskov, *Phys. Rev. B*, 1999, **60**, 6146–6154.

63   J. Greeley and M. Mavrikakis, *J. Phys. Chem. B*, 2005, **109**, 3460–3471.

64   L. Xu, H. Y. Xiao and X. T. Zu, *Chem. Phys.*, 2005, **315**, 155–160.

65   G. S. Karlberg, *Phys. Rev. B*, 2006, **74**, 153414.

66   W. P. Krekelberg, J. Greeley and M. Mavrikakis, *J. Phys. Chem. B*, 2004, **108**, 987–994.

67   G. Kresse and J. Hafner, *Surf. Sci.*, 2000, **459**, 287–302.

68   J. A. Herron, S. Tonelli and M. Mavrikakis, *Surf. Sci.*, 2012, **606**, 1670–1679.

69   D. C. Ford, Y. Xu and M. Mavrikakis, *Surf. Sci.*, 2005, **587**, 159–174.

70   J. L. Nie, H. Y. Xiao and X. T. Zu, *Chem. Phys.*, 2006, **321**, 48–54.

71   O. M. Lovvik and R. A. Olsen, *J. Chem. Phys.*, 2003, **118**, 3268–3276.

72   D. Vasic, Z. Ristanovic, I. Pasti and S. Mentus, *Russ. J. Phys. Chem. A*, 2011, **85**, 2373–2379.

73   B. Bhatia and D. S. Sholl, *J. Chem. Phys.*, 2005, **122**, 204707.

74   T. T. T. Hanh, Y. Takimoto and O. Sugino, *Surf. Sci.*, 2014, **625**, 104–111.

75   E. Vesselli, A. Baraldi, F. Bondino, G. Comelli, M. Peressi and R. Rosei, *Phys. Rev. B*, 2004, **70**, 3–8.

76   G. Pauer, A. Eichler, M. Sock, M. G. Ramsey, F. Netzer and A. Winkler, *J. Chem. Phys.*, 2003, **119**, 5253–5260.

77   D. Lerch, A. Klein, A. Schmidt, S. Müller, L. Hammer, K. Heinz and M. Weinert, *Phys. Rev. B*, 2006, **73**, 075430.

78   K. Heinz, L. Hammer, B. Gumler, W. Meyer and A. Schmidt, *Z. Phys. Chem.*, 2009, **223**, 75–88.

79   I. Stensgaard and F. Jakobsen, *Phys. Rev. Lett.*, 1985, **54**, 711–713.

80   M. J. Gladys, I. Kambali, M. A. Karolewski, A. Soon, C. Stampfl and D. J. O'Connor, *J. Chem. Phys.*, 2010, **132**, 024714.

81   F. Besenbacher, I. Stensgaard and K. Mortensen, *Surf. Sci.*, 1987, **191**, 288–301.

82   D. Y. Zemlyanov, M. Y. Smirnov and V. V. Gorodetskii, *Catal. Letters*, 1997, **43**, 181–187.

83   A. Hellman, K. Svensson and S. Andersson, *J. Phys. Chem. C*, 2014, **118**, 15773–15778.

84   L. J. Lauhon and W. Ho, *Phys. Rev. Lett.*, 2000, **85**, 4566–4569.

85   M. Foss, F. Besenbacher, C. Klink and I. Stensgaard, *Chem. Phys. Lett.*, 1993, **215**, 535–540.

86   S. C. Jung and M. H. Kang, *Phys. Rev. B*, 2005, **72**, 205419.

87   W. Z. Lai, D. Q. Xie, J. L. Yang and D. H. Zhang, *J. Chem. Phys.*, 2004, **121**, 7434–7439.

88   S. Hong and T. S. Rahman, *Phys. Rev. B*, 2007, **75**, 155405.

89   N. Kapur, J. Hyun, B. Shan, J. B. Nicholas and K. Cho, *J. Phys. Chem. C*, 2010, **114**, 10171–10182.

90   R. A. Olsen, S. C. Badescu, S. C. Ying and E. J. Baerends, *J. Chem. Phys.*, 2004, **120**, 11852–11863.

91   H. A. Michelsen, C. T. Rettner and D. J. Auerbach, *Surf. React.*, 1994, **34**, 185–237.

92   F. Healey, R. N. Carter, G. Worthy and A. Hodgson, *Chem. Phys. Lett.*, 1995, **243**, 133–139.

93   S. Küchenhoff, W. Brenig and Y. Chiba, *Surf. Sci.*, 1991, **245**, 389–400.

94   D. Halstead and S. Holloway, *J. Chem. Phys.*, 1990, **93**, 2859–2870.

95   M. J. Murphy and A. Hodgson, *J. Chem. Phys.*, 1998, **108**, 4199–4211.

96   M. J. Murphy and A. Hodgson, *J. Chem. Phys.*, 1998, **108**, 4199–4211.

97   P. B. Rasmussen, P. M. Holmblad, H. Christoffersen, P. A. Taylor and I. Chorkendorff, *Surf. Sci.*, 1993, **287-288**, 79–83.

98   T. Gomez, E. Florez, J. A. Rodriguez and F. Illas, *J. Phys. Chem. C*, 2011, **115**, 11666–11672.

99   A. Gross, B. Hammer, M. Scheffler and W. Brenig, *Phys. Rev. Lett.*, 1994, **73**, 3121–3124.

100   Y. Xu, J. Greeley and M. Mavrikakis, *J. Am. Chem. Soc.*, 2005, **127**, 12823–12827.

101   G. J. Kroes, A. Gross, E. J. Baerends, M. Scheffler and D. A. McCormack, *Acc. Chem. Res.*, 2002, **35**, 193–200.

102   A. Eichler, J. Hafner, A. Gross and M. Scheffler, *Phys. Rev. B*, 1999, **59**, 13297–13300.

$$TIE \equiv \frac{K_{eq}^{H}}{K_{eq}^{D}}$$
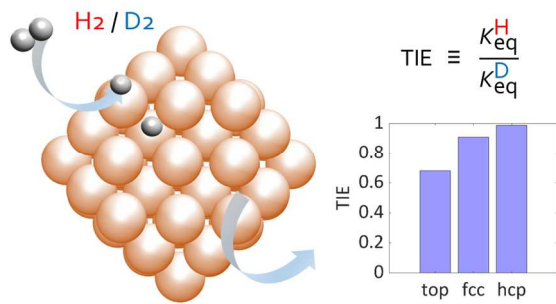
Thermodynamic/kinetic isotope effects for H_2/D_2 dissociative adsorption calculated on metal surfaces offer a means to identify active sites.